STING directly recruits WIPI2 for autophagosome formation during STING-induced autophagy

Wei Wan[1],[*] ID, Chuying Qian[1], Qian Wang[1], Jin Li[1] ID, Hongtao Zhang[1], Lei Wang[1], Maomao Pu[2], Yewei Huang[2], Zhengfu He[1], Tianhua Zhou[1] ID, Han-Ming Shen[3] ID & Wei Liu[1,2,4,][**] ID

Abstract

The cGAS-STING pathway plays an important role in host defense by sensing pathogen DNA, inducing type I IFNs, and initiating autophagy. However, the molecular mechanism of autophagosome formation in cGAS-STING pathway-induced autophagy is still unclear. Here, we report that STING directly interacts with WIPI2, which is the key protein for LC3 lipidation in autophagy. Binding to WIPI2 is necessary for STING-induced autophagosome formation but does not affect STING activation and intracellular trafficking. In addition, the specific interaction between STING and the PI3P-binding motif of WIPI2 leads to the competition of WIPI2 binding between STING and PI3P, and mutual inhibition between STING-induced autophagy and canonical PI3P-dependent autophagy. Furthermore, we show that the STING-WIPI2 interaction is required for the clearance of cytoplasmic DNA and the attenuation of cGAS-STING signaling. Thus, the direct interaction between STING and WIPI2 enables STING to bypass the canonical upstream machinery to induce LC3 lipidation and autophagosome formation.

Introduction

By recognizing microbial components, pattern recognition receptors (PRRs) initiate intracellular signaling to activate innate immunity. In mammalian cells, the DNA-sensing cyclic GMP-AMP (cGAMP) synthase (cGAS) functions as an intracellular PRR to trigger pathogen DNA-driven immune responses. This process relies on the binding of cGAMP to the adaptor protein stimulator of interferon genes (STING) and subsequently the export of STING from the endoplasmic reticulum (ER; Chen *et al*, 2016b; Motwani *et al*, 2019). The cGAS-STING pathway activates the synthesis of antiviral type I interferons (IFNs) through the TANK-binding kinase 1 (TBK1)-dependent transcription factor interferon regulatory factor 3 (IRF3), and of proinflammatory cytokines via NF-κB (Chen *et al*, 2016b; Motwani *et al*, 2019). Mice deficient in cGAS-STING signaling are susceptible to lethal infection by DNA viruses (Ishikawa *et al*, 2009; Li *et al*, 2013), highlighting the critical role of the cGAS-STING pathway in combating viral infection. However, the type I IFN response may also be used by pathogenic bacteria for their dissemination and to promote chronic persistent infections (McNab *et al*, 2015). Excessive or prolonged activation of cGAS-STING signaling is associated with a broad array of inflammatory and autoimmune diseases (Motwani *et al*, 2019; Ma *et al*, 2020).

Recent studies have indicated that cGAS-STING signaling also activates macroautophagy (hereafter referred to as autophagy; Watson *et al*, 2012, 2015; Liang *et al*, 2014; Prabakaran *et al*, 2018; Gui *et al*, 2019; Liu *et al*, 2019), the autophagosome- and lysosome-dependent intracellular degradation process, and induction of autophagy is a primordial function of the cGAS-STING pathway (Gui *et al*, 2019). Upon binding to cGAMP, STING translocates from the ER to the ER-Golgi intermediate compartment (ERGIC) and the Golgi complex via the COPII vesicle transport pathway (Gui *et al*, 2019). In both STING-induced autophagy and starvation-induced canonical autophagy, the ERGIC serves as a membrane source for LC3 lipidation and autophagosome formation (Ge *et al*, 2013; Gui *et al*, 2019). In STING-induced autophagy, activated STING drives the formation of these ERGIC-derived vesicles (Gui *et al*, 2019). Accumulating evidence has suggested that this STING-mediated autophagy is essential for not only the clearance of cytoplasmic DNA (Liang *et al*, 2014; Gui *et al*, 2019) but also the attenuation of the cGAS-STING signaling by selectively degrading cGAS and STING (Chen *et al*, 2016a; Prabakaran *et al*, 2018; Jena *et al*, 2020), and possibly the downstream IRF3 (Jiang *et al*, 2018; Wu *et al*, 2021). This ensures the precise control of IRF3 activity and type I IFN production, thereby fine-tuning the immune response.

The core autophagy machinery proteins autophagy protein 5 (ATG5) and WIPI2, a phosphatidylinositol-3-phosphate (PI3P)- and ATG16L1-binding protein, are crucial for cGAMP-stimulated LC3

1   Department of Biochemistry, and Department of Thoracic Surgery of Sir Run Run Shaw Hospital, Zhejiang University School of Medicine, Hangzhou, China
2   Department of Metabolic Medicine, International Institutes of Medicine, the Fourth Affiliated Hospital, Zhejiang University School of Medicine, Yiwu, China
3   Faculty of Health Sciences, University of Macau, Macau, China
4   Joint Institute of Genetics and Genomics Medicine between Zhejiang University and University of Toronto, Hangzhou, China
   *Corresponding author. Tel: +86 571 8820 8551; E-mail: wanwei@zju.edu.cn
   **Corresponding author. Tel: +86 571 8820 8357; E-mail: liuwei666@zju.edu.cn

lipidation and autophagosome formation (Gui et al, 2019). Intriguingly, a number of autophagy-related proteins that are required for canonical autophagy, including ATG9A, unc-51 like autophagy activating kinase 1 (ULK1) complex, and phosphatidylinositol 3-kinase catalytic subunit type 3 (PIK3C3/VPS34) complex, are not essential for STING-induced autophagy (Gui et al, 2019; Liu et al, 2019). Of these proteins and protein complexes, the most notable is the PIK3C3 complex, due to the key role of its product PI3P in the formation and expansion of phagophores, either from the omegasomes or the ERGIC (Dooley et al, 2014; Ge et al, 2014). For the former, PI3P recruits the ATG12-ATG5-ATG16L1 complex via WIPI2 to target LC3 to the phagophore (Polson et al, 2010; Dooley et al, 2014); For the latter, PI3P collects COPII proteins to generate vesicles from the ERGIC (Ge et al, 2014; Davis et al, 2016). Numerous studies have proved that WIPI2 plays an indispensable role in canonical autophagy (Polson et al, 2010; Dooley et al, 2014; Zhao et al, 2017; Wan et al, 2018; Lu et al, 2019; Fracchiolla et al, 2020). The cGAS-STING pathway-induced autophagy requires WIPI2 but not PIK3C3 complex, indicating the existence of a PI3P-independent mechanism for the membrane recruitment of WIPI2.

In this study, we have performed mass spectrometry analysis of STING vesicles to screen for proteins that may participate in cGAS-STING pathway-induced autophagy. Among the proteins, we find that WIPI2 and its interacting partner ATG16L1 are enriched in STING vesicles. By identifying WIPI2 as a constitutive STING-binding protein, we elucidate that the direct interaction between WIPI2 and STING enables WIPI2 to target STING-positive vesicles for LC3 lipidation and autophagosome formation during STING-induced autophagy. Moreover, we provide evidence that this PI3P-independent mobilization of WIPI2 is necessary for the autophagic clearance of cytoplasmic DNA and the attenuation of activated cGAS-STING signaling.

Results

WIPI2 is recruited to STING vesicles

Given that STING-containing vesicles derived from the ERGIC act as the primary membrane source for autophagosome formation during STING-induced autophagy (Gui et al, 2019; Liu et al, 2019), we speculated that specific proteins participating in the autophagosome formation process may be localized to STING vesicles. Therefore, we set up a STING-positive membrane isolation assay in HEK293T cells stably expressing STING-HA (Fig 1A). Cells were treated with cGAMP and then homogenized in the absence of detergent. After incubation with anti-HA affinity beads, the beads-bound STING-positive membranes were precipitated and subjected to mass spectrometry analysis. High abundance proteins dragged down by STING-positive membranes included TBK1, SQSTM1, and SEC24C (Fig 1B and Dataset EV1), three known STING-binding proteins (Prabakaran et al, 2018; Gui et al, 2019). Interestingly, WIPI2 and its binding partner ATG16L1, and many other autophagy-related proteins including ATG5, ATG12, LC3, and NBR1, were also among the proteins (Fig 1B and Dataset EV1). In addition, many proteins identified in STING-positive membranes were recently shown to have an affinity with STING by a proximity labeling screen using STING as bait (Chu et al, 2021; Dataset EV1). To verify the

localization of WIPI2 in STING vesicles, we performed a western blot analysis on the isolated STING-positive membranes. WIPI2 and ATG16L1 but not WIPI1, another PI3P-binding member of the WIPI family, were precipitated by the STING-positive membranes, and the precipitation was unaffected by TBK1/IKKε inhibitor BX795 (Appendix Fig S1A). We also observed the distribution of transfected WIPI2-GFP in HEK293T cells stably expressing STING-HA. Upon cGAMP treatment, co-localization of WIPI2-GFP with STING-HA puncta was detected (Fig 1C and D). Endogenous WIPI2 also co-localized with endogenous STING puncta in cGAMP-treated mouse embryonic fibroblasts (MEFs; Fig 1E and F). In addition, cGAMP stimulation led to the localization of endogenous ATG16L1 to the STING-HA puncta (Fig 1G and H). Using a specific antibody against ERGIC-53, a marker protein of the ERGIC, in MEFs, we detected an overlap between WIPI2-GFP and ERGIC-53, which was more obvious at the puncta surrounding the ERGIC body (Appendix Fig S1B and C). By contrast, GFP-tagged WIPI1 was not found in STING puncta (Fig 1I). This suggests that WIPI2 undergoes a specific and PI3P-independent association with STING vesicles. In support of this, neither GFP-tagged ATG14L, a constitutive subunit of PIK3C3 complex 1, nor DFCP1, an omegasome marker protein that binds to PI3P, was detected in the puncta (Appendix Fig S1D–G). Finally, using a STING mutant (STING-R238A) that is incapable of cGAMP binding, we confirmed that, in cGAMP-treated cells, the redistribution of WIPI2 relies on the activation and translocation of STING (Fig 1J). Taken together, these results suggest that WIPI2 can be recruited to cGAMP-stimulated STING vesicles through a PI3P-independent manner.

WIPI2 directly interacts with STING

Next, we explored the mechanism by which WIPI2 is specifically recruited to STING vesicles. A simple hypothesis is that WIPI2 is a STING-binding protein. Interestingly, immunoprecipitation of WIPI2-Myc but not WIPI1-Myc co-precipitated endogenous STING from transfected MEFs, and cGAMP treatment did not increase the co-precipitation (Fig 2A). To determine where STING-WIPI2 interaction occurs, we fractionated cell membranes of HEK293T cells stably expressing STING-HA with or without cGAMP stimulation. After differential centrifugation followed by sucrose gradient and Opti-Prep density-gradient ultracentrifugation, membrane fractions were collected, diluted, and subjected to immunoprecipitation (Fig EV1A). In cells with or without cGAMP treatment, STING and WIPI2 were strongly distributed in the ERGIC and the ER membrane fractions and they interacted there, respectively (Fig EV1B). Interestingly, STING but not WIPI2 was detected in the endosome/lysosome fractions of cGAMP-stimulated cells (Fig EV1B). Of note, in cells treated with brefeldin A, which inhibits ER-to-Golgi trafficking and abolishes STING vesicle formation (Gui et al, 2019), the STING-WIPI2 interaction was unaffected (Fig EV1C). Unlike mouse WIPI2, which has only one isoform, human WIPI2 has different isoforms (Dooley et al, 2014; Wan et al, 2018). We found that all four tested human WIPI2 isoforms could be co-immunoprecipitated by STING-HA (Fig EV1D). Moreover, STING-R238A, which cannot bind cGAMP, and STING-S366A, which cannot lead to IRF3 phosphorylation and activation (Gui et al, 2019), co-precipitated with WIPI2 at a similar level as wild-type (WT) STING (Fig 2B). These results strongly suggest a constitutive
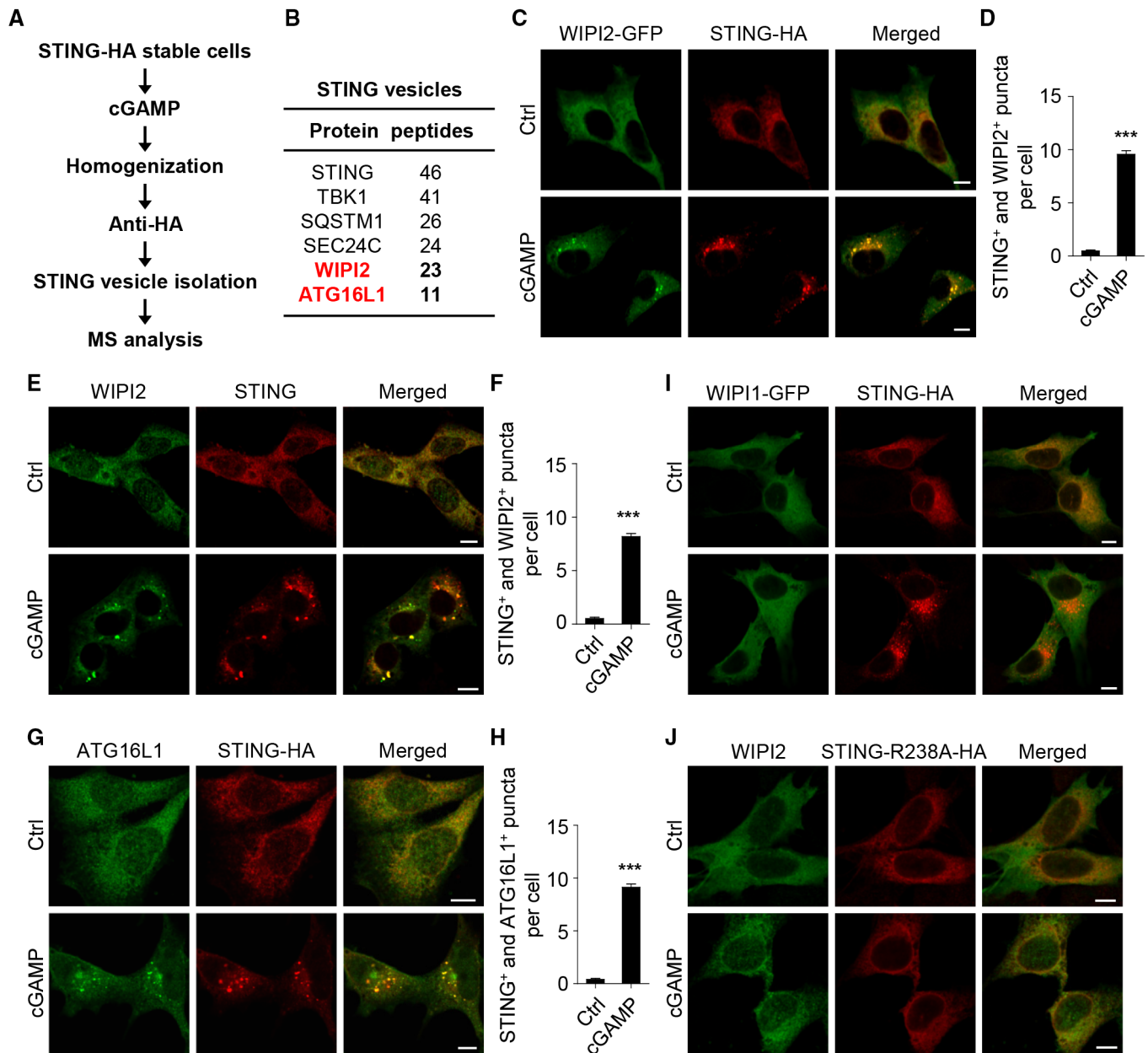
Figure 1. WIPI2 is recruited to STING vesicles.

A   Schematic of the workflow for identifying proteins those associated with STING vesicles. HEK293T cells stably expressing STING-HA were treated with cGAMP and homogenized in extraction buffer without detergent. After incubation with anti-HA affinity beads, STING vesicles were isolated and subjected to mass spectrometry analysis.

B   Some of the highly abundant proteins in isolated STING vesicles.

C   Distribution of WIPI2-GFP in HEK293T cells stably expressing STING-HA. The cells were transfected with WIPI2-GFP.

D   Statistical analysis of the number of STING- and WIPI2-positive puncta in cells treated as in (C).

E   Distribution of endogenous WIPI2 and STING in MEFs.

F   Statistical analysis of the number of STING- and WIPI2-positive puncta in cells treated as in (E).

G   Distribution of endogenous ATG16L1 in HEK293T cells stably expressing STING-HA.

H   Statistical analysis of the number of STING- and ATG16L1-positive puncta in cells treated as in (G).

I, J   Distribution of WIPI1-GFP in HEK293T cells stably expressing STING-HA (I) and endogenous WIPI2 in HEK293T cells stably expressing STING-R238A-HA (J).

Data information: All the cells were treated with or without cGAMP for 2 h. All statistical data are presented as mean $\pm$ SEM of three independent experiments. $n = 60$.
***$P < 0.001$ (Student's t-test). Scale bars, 10 µm.
Source data are available online for this figure.

binding of WIPI2 to STING, independent of STING trafficking and activation.

To further clarify the interaction between STING and WIPI2, we constructed truncated WIPI2 mutants and found that the region containing amino acid 215–259 in WIPI2 was required for STING binding (Fig 2C). In addition, we created GFP-tagged truncated WIPI2s (amino acid 215–259 and 260–301) and examined their affinities for STING. The result revealed that amino acid 215–259 is sufficient to mediate WIPI2 interaction with STING (Fig 2D). The FRRG motif that mediates the binding of WIPI2 to PI3P is located in this region (Polson et al, 2010; Dooley et al, 2014). Therefore, we tested whether the same motif of WIPI2 is also required for STING-WIPI2 interaction. By replacing the two arginine residues in the FRRG motif with threonine or lysine, we generated WIPI2-FTTG and WIPI2-FKKG mutants that are incapable of PI3P binding (Polson et al, 2010; Lu et al, 2011; Dooley et al, 2014). Interestingly, WIPI2-FKKG, or WIPI2-R108E/R125E mutant, which cannot bind to ATG16L1 (Dooley et al, 2014) but not WIPI2-FTTG interacted with STING (Fig 2E and F), which suggests that the positively charged basic amino acid residues within the FRRG motif are important. Meanwhile, the WIPI2-FKKG mutant showed even higher affinity for STING than WT WIPI2 (Fig 2E and F).

We then tried to locate the sites in STING that mediate STING-WIPI2 interaction. Using a similar approach, we found that the region containing amino acid 277–334 in STING was required for STING to interact with WIPI2 (Figs 2G and EV1E). Considering the role of the two basic arginine residues in the FRRG motif of WIPI2, we speculated that acidic amino acids are needed in STING. Based on the known structure of human STING (Ramanjulu et al, 2018), we identified two acidic amino acid-rich motifs in the region 277–334: E282/D283/E286 (motif 1) and E296/D297/D301 (motif 2; Fig EV1F). We replaced the acidic residues with alanine to create two mutants, STING-3A-1 (E282A/D283A/E286A) and STING-3A-2 (E296A/D297A/D301A), respectively. Co-immunoprecipitation experiments showed that STING-3A-2 co-precipitated less WIPI2 than WT STING and STING-3A-1 (Fig 2H and I). We also performed in vitro pull-down assays using purified truncated STING and full-length WIPI2. The binding of truncated STING to WIPI2 was markedly reduced by the FRRG>FTTG mutation in WIPI2 or by the E296A/D297A/D301A (3A-2) mutation in STING (Fig 2J and K).

Binding of WIPI2 to STING is necessary for STING-induced autophagy

We then investigated the role of WIPI2 and STING-WIPI2 interaction in STING-induced autophagy. First, we found that, in cGAMP-treated cells, WT WIPI2 formed punctate structures similar to those in Torin1-treated cells (Fig 3A and B). We also observed that WIPI2-FKKG (which can bind STING but not PI3P), formed puncta only in cGAMP-treated cells, while WIPI2-FTTG (which interacts with neither STING nor PI3P), failed to form puncta in both cGAMP-treated cells and Torin1-treated cells (Fig 3A and B). In addition, consistent with previous studies (Dooley et al, 2014; Gui et al, 2019), knockout of Wipi2 significantly decreased the production of LC3-II in cGAMP-treated cells and Torin1-treated cells (Fig 3C). Re-transfection of WIPI2-FKKG but not WIPI2-FTTG rescued cGAMP-induced but not Torin1-induced LC3-II formation (Fig 3C).

cGAMP treatment failed to induce the formation of LC3 puncta in WT HEK293T cells (Appendix Fig S2A and B), as STING is silenced in these cells (Sui et al, 2017; Gui et al, 2019). We therefore established stable cell lines by transfecting HA-tagged WT STING or STING mutants into STING-deficient HEK293T cells and examined the formation of autophagosomes in these cells. cGAMP treatment did not induce the formation of LC3 puncta in cells expressing STING-3A-2, which cannot bind to WIPI2, or in cells expressing STING-R238A, which cannot be activated by cGAMP (Fig 3D and E). Consistent with this, cGAMP-induced LC3-II formation and p62 degradation were much weaker or absent in these cells when compared with cells expressing WT STING (Fig 3F). In MEFs stably expressing GFP-LC3, cGAMP treatment resulted in the localization of endogenous WIPI2 and STING to formed GFP-LC3 puncta (Fig EV2A and B) and knockout of Wipi2 inhibited the formation of LC3 puncta (Fig EV2C and D). Previously, it was reported that STING induces LC3 lipidation and autophagy by binding LC3 through LC3-interacting regions (LIRs; Liu et al, 2019). We found that mutation of all the LIRs, located in the c-di-GMP-binding domain (CBD) of STING (Liu et al, 2019), did not influence STING-WIPI2 interaction (Appendix Fig S2C). Unexpectedly, the STING mutant with disrupted LIRs was unable to form puncta in cGAMP-treated cells (Appendix Fig S2D), suggesting that they are required for STING trafficking. Taken together, these results suggest that interaction

Figure 2. WIPI2 directly interacts with STING.

A   Co-immunoprecipitation of endogenous STING with WIPI1/2-Myc in MEFs transfected with Myc-tagged WIPI1 or WIPI2. The cells were treated with or without cGAMP for 2 h and the WIPI1/2-Myc precipitates were analyzed by western blot using anti-STING.

B   Co-immunoprecipitation of endogenous WIPI2 with HA-tagged STING, STING-R238A, or STING-S366A from HEK293T cells stably expressing STING-HA, STING-R238A-HA or STING-S366A-HA. The cells were treated with or without cGAMP for 2 h.

C–E Co-immunoprecipitation of endogenous STING with Myc- or GFP-tagged WIPI2 or the indicated WIPI2 mutants from MEFs transfected with the indicated plasmids.

F   Statistical analysis of (E).

G, H Co-immunoprecipitation of endogenous WIPI2 with HA-tagged STING or the indicated STING mutants from HEK293T cells transfected with the indicated plasmids. 3A-1, E282, D283 and E286 were replaced by alanine; 3A-2, E296, D297 and D301 were replaced by alanine.

I   Statistical analysis of (H).

J   Purified GST-tagged STING-153-379 or STING-153-379-3A-2 was incubated with recombinant WIPI2 or the indicated WIPI2 mutants and then precipitated with glutathione-sepharose beads. The bound WT or mutant WIPI2 was detected by western blot using anti-WIPI2.

K   Statistical analysis of (J).

Data information: All statistical data are presented as mean ± SEM of three independent experiments. *P < 0.05, **P < 0.01 (Student's t-test).
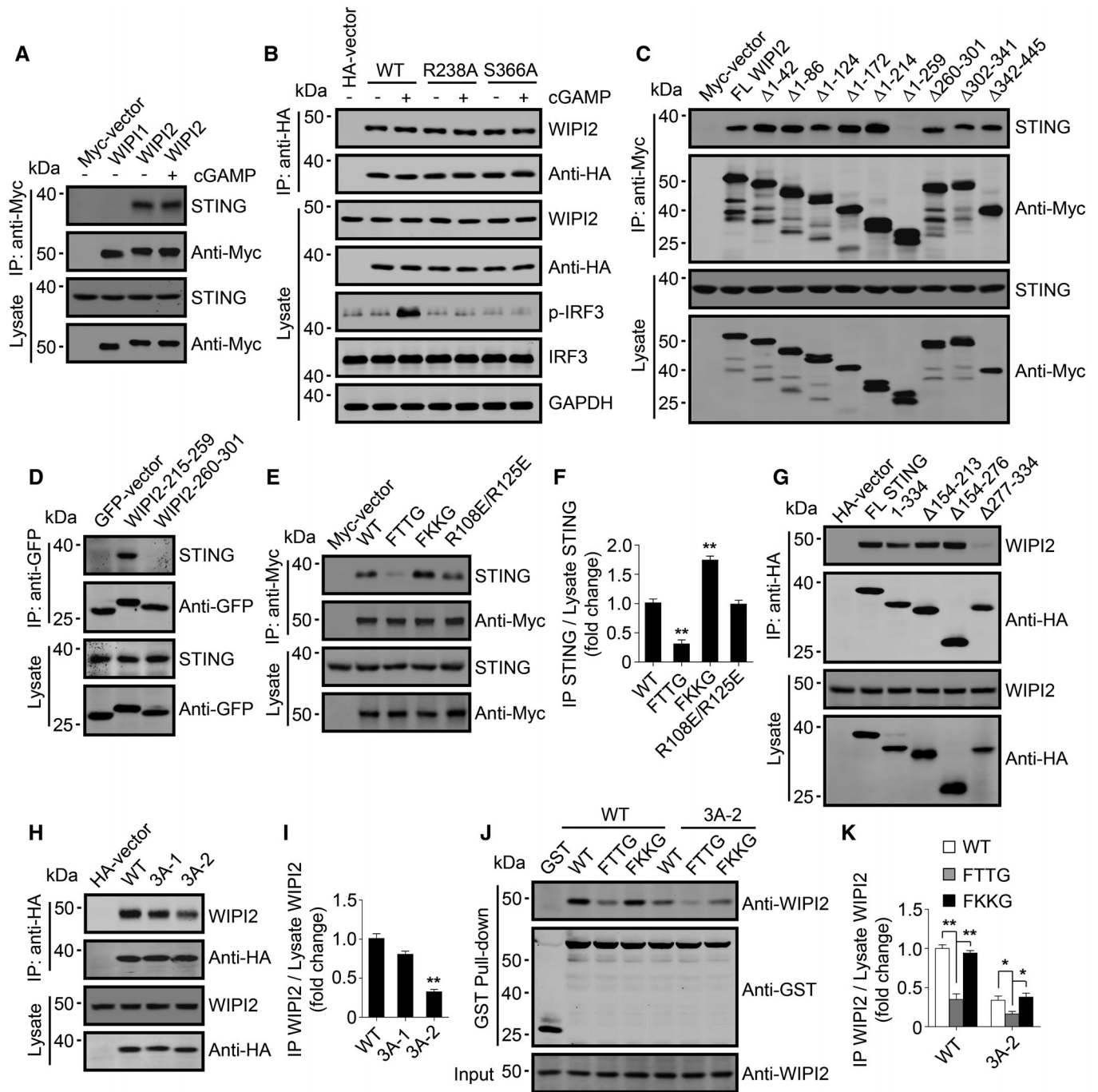Source data are available online for this figure.

Figure 2.

with WIPI2 is required for STING to induce LC3 lipidation and autophagosome formation.

In MEFs, *Wipi2* knockout showed no effect on cGAMP-stimulated STING punctum formation and TBK1 phosphorylation (Appendix Fig S2E and F). In addition, in HEK293T cells expressing STING-3A-2, cGAMP treatment resulted in the formation of STING-3A-2 puncta, the phosphorylation of TBK1, and the co-localization of phospho-TBK1 with STING-3A-2 puncta (Appendix Fig S2G). These data suggest that STING-WIPI2 interaction is unnecessary for STING trafficking and TBK1 activation.

Recently, it has been reported that STING can induce LC3 lipidation onto single-membrane vesicles (Fischer *et al*, 2020). Therefore, in our study, we examined whether STING-induced LC3 lipidation is also indeed involved in the formation of autophagosomes. In cGAMP-treated cells, syntaxin 17 (STX17), an autophagosomal SNARE (Itakura *et al*, 2012), was co-localized with LC3 on STING puncta (Appendix Fig S3A). This suggests that these STING- and LC3-positive puncta may represent double-membrane autophagosomes. Because p62 can interact with STING and might be engulfed into STING-induced autophagosomes (Prabakaran
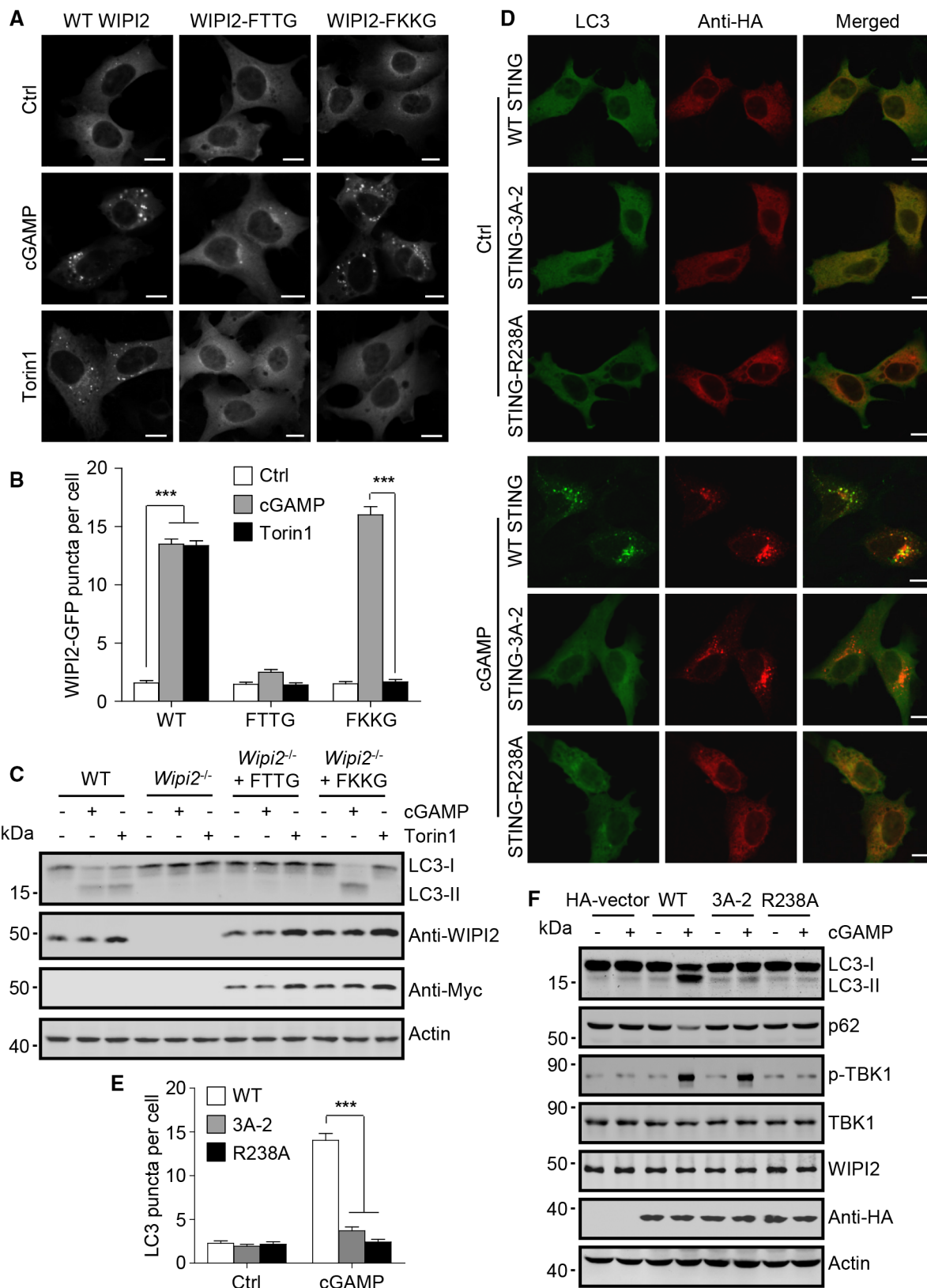
Figure 3.

◄

Figure 3. Binding of WIPI2 to STING is necessary for STING-induced autophagy.

A   WIPI2-GFP puncta in MEFs stably expressing GFP-tagged WT or mutant WIPI2. The cells were treated with cGAMP for 2 h or Torin1 for 1 h.
B   Statistical analysis of the number of WIPI2-GFP puncta in cells treated as in (A).
C   Western blot assay of LC3 in *Wipi2*-KO MEFs with or without re-introduction of the indicated WIPI2 mutants. The cells were treated with or without cGAMP for 2 h or Torin1 for 1 h.
D   Localization of LC3 in HEK293T cells stably expressing HA-tagged WT or mutant STING. The cells were treated with or without cGAMP for 2 h.
E   Statistical analysis of the number of LC3 puncta in cells treated as in (D).
F   LC3 and p62 level in HEK293T cells stably expressing HA-tagged WT or mutant STING. The cells were treated with or without cGAMP for 4 h.

Data information: All statistical data are presented as mean ± SEM of three independent experiments. $n = 60$. ***$P < 0.001$ (Student's *t*-test). Scale bars, 10 μm.
Source data are available online for this figure.

---

et al, 2018), we further performed a p62 protease protection assay (Valverde *et al*, 2019; Ohnstad *et al*, 2020; Appendix Fig S3B). We found that p62 was contained in STING-positive membranes pulled down from WT MEFs and *Atg5*-KO MEFs (Appendix Fig S3C). After treating the membranes with trypsin, p62 protein was not detectable in the membranes from *Atg5*-KO cells, but it was still present in the membranes from WT MEFs (Appendix Fig S3C). This indicated that a portion of p62 was included within double-membrane autophagosomes and protected from proteolysis. Using the same methods, similar results were obtained in membranes from *Wipi2*-KO cells, and the re-introduction of WIPI2-FKKG but not WIPI2-FTTG into *Wipi2*-KO cells protected p62 from proteolysis (Appendix Fig S3D). Since the C-terminal WD40 domain (WDD) of ATG16L1 is crucial for the lipidation of LC3 on single-membrane STING vesicles rather than double-membrane autophagosomes (Fletcher *et al*, 2018; Fischer *et al*, 2020), we examined the role of the WDD in the recruitment of ATG16L1 to STING puncta. We created Myc-tagged truncated ATG16L1 without WDD (amino acid 1–336) and found that this mutant was still able to be recruited to STING puncta in cGAMP-treated cells (Appendix Fig S3E). However, further mutation at the WIPI2-binding sites (E226R/E230R) completely eliminated the recruitment (Dooley *et al*, 2014; Appendix Fig S3E), confirming that ATG16L1 is able to be recruited to STING-positive membranes through a WIPI2-dependent manner. Taken together, these results suggest that STING-bound WIPI2 is required for STING-induced autophagy.

PI3P and STING compete for WIPI2, resulting in mutual inhibition between canonical autophagy and STING-induced autophagy

Both PI3P and STING bind to the FRRG motif of WIPI2, suggesting that intracellular PI3P and STING may compete for WIPI2. We examined STING-WIPI2 interaction in cells subjected to starvation or Torin1 treatment, both of which activate PIK3C3 complex 1 and induce canonical autophagy. In HEK293T cells stably expressing STING-HA, co-immunoprecipitation showed that starvation or Torin1 treatment reduced STING-WIPI2 binding (Fig 4A and B). By contrast, treatment of the cells with VPS34-IN1, a specific PIK3C3 complex inhibitor (Bago *et al*, 2014), increased the binding and reversed the decreased binding caused by starvation or Torin1 treatment (Fig 4A and B). Because intracellular WIPI2 protein levels increased in starved or Torin1-treated cells, consistent with our previous study (Wan *et al*, 2018), we also chose to pretreat cells with MG132 to stabilize intracellular WIPI2 and then conducted the co-immunoprecipitation analysis. Consistent results were obtained by detecting STING-WIPI2 binding (Appendix Fig S4A and B). Since WIPI2 can be phosphorylated by mTORC1 at Ser395 and this phosphorylation affects the stability of WIPI2 (Wan *et al*, 2018), we tested whether mTORC1-mediated phosphorylation directly affects STING-WIPI2 interaction. Like WT WIPI2, phosphorylation-disabled (S395A) and phosphorylation-mimicking (S395D) WIPI2 mutants were similarly co-precipitated with STING from cells treated with or without Torin1 (Appendix Fig S4C and D). Deletion of *BECN1*, an essential subunit of PIK3C3 complex, enhanced STING-WIPI2

Figure 4. PI3P negatively regulates STING-induced autophagy.

A   Co-immunoprecipitation of endogenous WIPI2 with STING-HA from HEK293T cells stably expressing STING-HA. The cells were pretreated with or without VPS34-IN1 for 1 h and then starved or treated with Torin1 for another 3 h along with VPS34-IN1. ST, starvation.
B   Statistical analysis of (A).
C   Co-immunoprecipitation of endogenous WIPI2 with STING-HA from HEK293 cells stably expressing STING-HA with or without *BECN1* deletion. The cells were treated with or without Torin1 for 3 h.
D   Statistical analysis of (C).
E   Co-immunoprecipitation of endogenous STING with Myc-tagged WT or mutant WIPI2 from MEFs treated with or without VPS34-IN1 for 2 h.
F   Statistical analysis of (E).
G   GFP-LC3 punctum formation in MEFs stably expressing GFP-LC3 and STING-HA. The cells were treated with or without cGAMP or VPS34-IN1 for 2 h. Scale bars, 10 μm.
H   Statistical analysis of the number of GFP-LC3 puncta in cells treated as in (G). $n = 60$.
I   Western blot assay of p62 and phospho-TBK1 (Ser172) in MEFs. The cells were pretreated with or without VPS34-IN1 for 1 h and then co-treated with cGAMP or Torin1 for another 4 h along with or without CQ. CQ, chloroquine.
J   Statistical analysis of p62 protein level in cells treated as in (I).

Data information: All statistical data are presented as mean ± SEM of three independent experiments. *$P < 0.05$, **$P < 0.01$, ***$P < 0.001$ (Student's *t*-test).
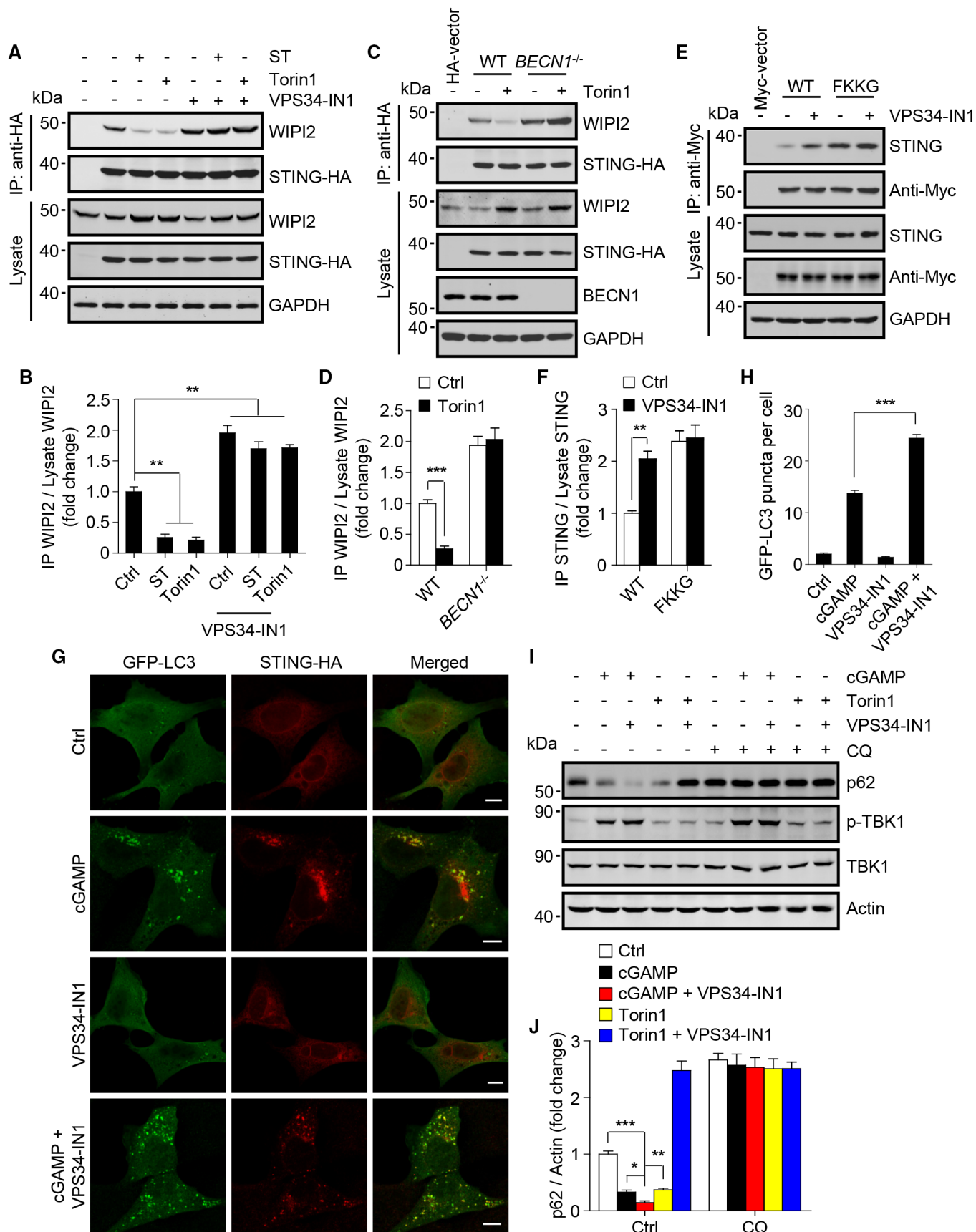Source data are available online for this figure.

▶

Figure 4.

interaction and prevented the effect of Torin1 (Fig 4C and D). Interestingly, WIPI2-FKKG, unable to bind PI3P, showed a higher interaction with STING, and this interaction was unaffected by VPS34-IN1 treatment (Fig 4E and F). Furthermore, in PI3P-rich membranes isolated from starved or Torin1-treated cells stably expressing HA-DFCP1 (Judith *et al*, 2019; Appendix Fig S4E), WIPI2 and WIPI1, but not STING, were contained in the membranes (Appendix Fig S4F). Finally, by incubating STING-HA precipitates with PI3P- or PI-decorated liposomes, we found that PI3P but not PI was able to dissociate WIPI2 from STING (Appendix Fig S4G and H). Taken together, these results suggest that PI3P negatively regulates STING-WIPI2 interaction.

We then checked the effect of intracellular PI3P on STING-induced autophagy in cells stably expressing GFP-LC3 and STING-HA. Interestingly, while VPS34-IN1 treatment itself almost had no effect on the formation of GFP-LC3 puncta, it significantly increased the number of cGAMP-stimulated GFP-LC3 puncta (Fig 4G and H). To confirm that VPS34-IN1 treatment itself does influence the basal level of autophagy, we examined the protein levels of autophagy receptors p62 and NBR1. VPS34-IN1 treatment increased p62 and NBR1 proteins in WT but not *BECN1*-deficient cells (Fig EV3A and B), indicating that VPS34-IN1 inhibits the production of PI3P in cells under basal condition. In addition, VPS34-IN1 treatment also completely eliminated the formation of GFP-DFCP1 puncta induced by starvation (Fig EV3C and D), confirming the inhibitory effect of VPS34-IN1 on PI3P synthesis in cells. Consistent with the inhibitory effect on PI3P-dependent autophagy, VPS34-IN1 treatment blocked the reduction in p62 protein level induced by Torin1, while it promoted the reduction in p62 protein level induced by cGAMP (Fig 4I and J). Treatment of cells with chloroquine (CQ), a lysosome inhibitor, prevented all the decreases, which suggests that they were caused by lysosome-dependent degradation (Fig 4I and J).

We also tested the potential effect of STING on canonical autophagy. Deletion of *Sting* in MEFs significantly increased the number of GFP-LC3 puncta in CQ-treated or untreated cells (Fig EV3E and F). In addition, deletion of *Sting* reduced the cellular p62 protein level and further promoted the degradation of p62 triggered by starvation or Torin1 treatment (Fig EV3G and H). Together, these data suggest that there is a reciprocal inhibition between STING-mediated noncanonical autophagy and PI3P-dependent canonical autophagy.

STING-WIPI2 interaction is required for cytoplasmic DNA clearance

We next assessed the physiological effect of STING-WIPI2 interaction by examining the clearance of cytoplasmic DNA. First, in MEFs transfected with Cy3 labeled-interferon stimulatory DNA (ISD), we found that endogenous WIPI2 and ATG16L1, but not WIPI1, were localized to Cy3-ISD puncta (Figs 5A and EV4A). Using arabinofuranosyl cytidine (Ara-C), a chemical that interferes with DNA synthesis and leads to DNA damage (Grant, 1998), we observed that WIPI2 encapsulated endogenous cytoplasmic DNA (Fig EV4B). While both WIPI2 and LC3 were localized to Cy3-ISD puncta (Fig EV4C), knockout of *Wipi2* significantly reduced the co-localization of LC3 with Cy3-ISD puncta (Fig EV4D and E). Of note, deletion of *Sting* but not *TBK1* eliminated the co-localization of WIPI2 with Cy3-ISD puncta (Fig EV4F and G). In addition, WIPI2-FKKG but not WIPI2-FTTG co-localized with Cy3-ISD puncta in MEFs (Figs 5B and EV4H). These results indicate that STING and STING-WIPI2 interaction but not TBK1 is required for the recruitment of WIPI2 to cytoplasmic DNA puncta.

We then evaluated the clearance of cytoplasmic DNA from cells. Co-treatment of cells with cGAMP significantly decreased Ara-C-stimulated accumulation of cytoplasmic DNA in WT but not *Wipi2*-KO MEFs (Fig 5C and D). In addition, re-introduction into these *Wipi2*-KO MEFs of WT WIPI2 or WIPI2-FKKG, but not WIPI2-FTTG or WIPI2-R108E/R125E (2RE), that is unable to interact with ATG16L1 (Dooley *et al*, 2014), reduced the accumulation of cytoplasmic DNA (Fig 5C and D). Consistent effects were observed in the clearance of exogenous Cy3-ISD (Appendix Fig S5A and B). In addition, we measured the level of intracellular cGAMP, synthesized when cGAS bind to cytoplasmic DNA. Obviously, knockout of *Wipi*2 further raised the cGAMP level in MEFs transfected with ISD (Appendix Fig S5C). Re-introduction of WT WIPI2 or WIPI2-FKKG but not WIPI2-FTTG abolished the increase in cGAMP level (Appendix Fig S5C). Furthermore, VPS34-IN1 treatment significantly promoted the clearance of cytoplasmic endogenous or exogenous DNA in cGAMP-stimulated cells (Fig 5E and F; Appendix Fig S5D and E). Taken together, these data suggest that STING-WIPI2 interaction plays an important role in STING-mediated clearance of cytoplasmic DNA, and the effect can be enhanced by inhibiting the production of intracellular PI3P.

Role of STING-WIPI2 interaction in attenuating activated cGAS-STING signaling

We also explored the role of WIPI2 and STING-WIPI2 interaction in the attenuation of cGAS-STING signals. Ara-C-treatment induced TBK1 phosphorylation and *Ifnb1* expression in WT but not *Sting*-KO cells (Fig 6A–C). Interestingly, Ara-C stimulated higher TBK1 phosphorylation and *Ifnb1* expression in *Wipi2*-KO cells than in WT cells

---

Figure 5. STING-WIPI2 interaction is required for cytoplasmic DNA clearance.

A, B   Localization of endogenous WIPI2, WIPI1, ATG16L1 (A) or Myc-tagged WT WIPI2 or WIPI2 mutants (B) in MEFs transfected with Cy3 labeled-ISD (1 μg/ml). ISD, interferon stimulatory DNA.

C   WT or *Wipi2*-KO MEFs stably expressing Myc-tagged WT WIPI2 or WIPI2 mutants were treated with Ara-C for 12 h and then stimulated with cGAMP for another 12 h. Cytoplasmic DNA was stained with a specific antibody against double-stranded DNA. Low-permeabilization buffer was used to allow the antibody to cross the cellular but not the nuclear membrane. 2RE, WIPI2-R108E/R125E; Ara-C, arabinofuranosyl cytidine.

D   Statistical analysis of cytoplasmic DNA puncta in cells treated as in (C).

E   PI3P inhibits cytoplasmic DNA clearance induced by cGAMP. MEFs were treated with Ara-C for 12 h and then stimulated with cGAMP, VPS34-IN1, or cGAMP and VPS34-IN1, for another 12 h.

F   Statistical analysis of cytoplasmic DNA puncta in cells treated as in (E).

Data information: All statistical data are presented as mean ± SEM of three independent experiments. *n* = 60. ***$P < 0.001$ (Student's *t*-test). Scale bars, 10 μm.
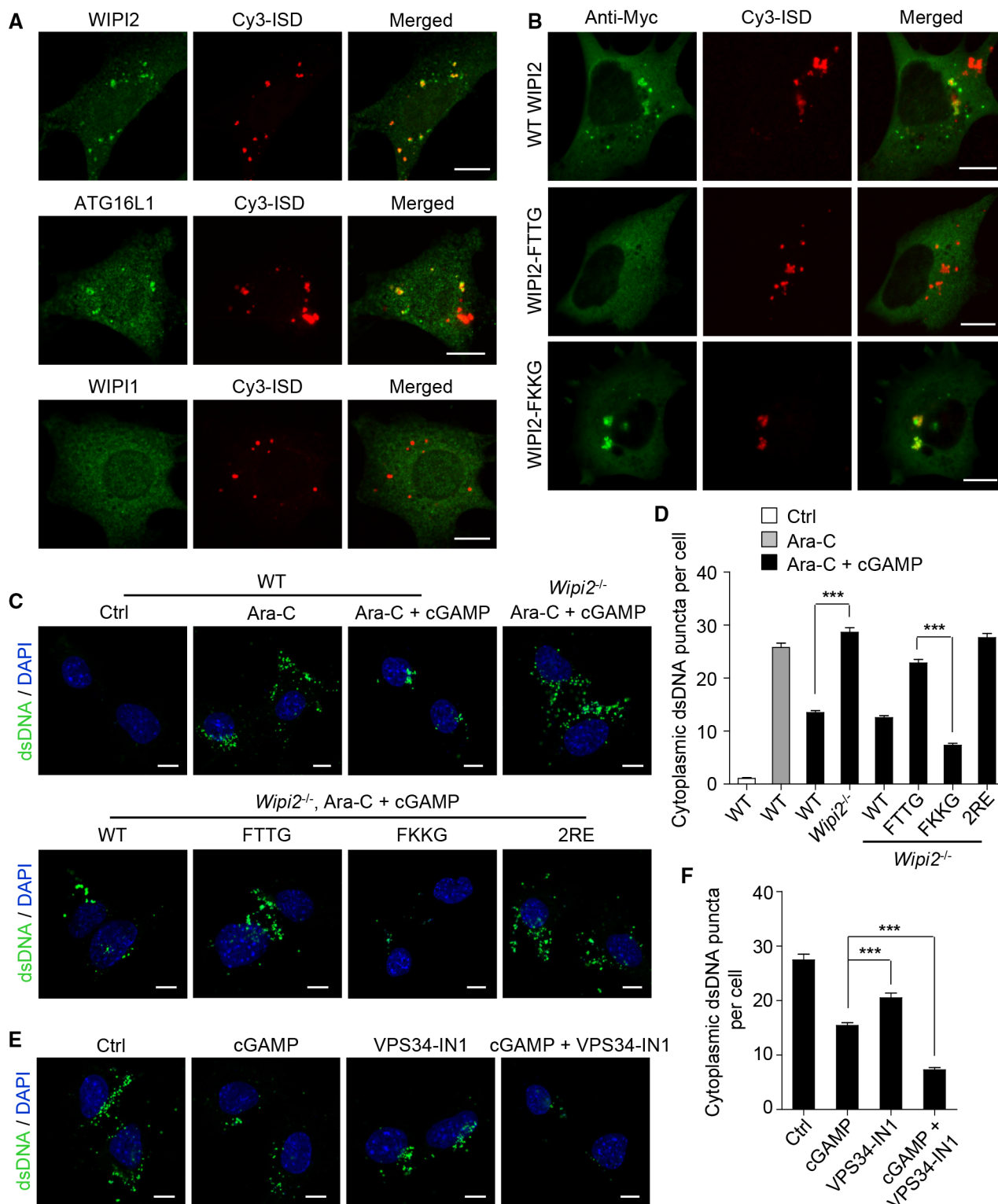Source data are available online for this figure.

Figure 5.

(Fig 6A–C). Removal of Ara-C from the culture medium significantly reduced the phosphorylation of TBK1 and expression of *Ifnb1* in WT but not *Wipi2*-KO cells (Fig 6A–C). Of note, the protein level of STING significantly decreased after Ara-C treatment and its removal

in WT cells but remained almost unchanged in *Wipi2*-KO cells (Fig 6A and B), confirming that STING itself is also a substrate of autophagy (Prabakaran *et al*, 2018). In addition, ISD transfection or cGAMP treatment decreased the protein level of STING in WT but

not *Wipi2*-KO cells (Fig EV5A and B). We also evaluated the role of WIPI2 in cGAS-STING signaling using primary human cells. In human monocyte-derived macrophages, knockdown of *WIPI2* further promoted ISD-induced phosphorylation of TBK1 and IRF3 and the expression of *IFNB1* (Fig EV5C–E). Meanwhile, ISD-induced degradation of STING was impaired in these cells (Fig EV5C and D). These data suggest that deletion of *Wipi2* disrupts the attenuation of cGAS-STING signaling after its activation. We further examined the *Ifnb1* mRNA level in *Wipi2*-KO cells after re-introduction of WT WIPI2 or WIPI2 mutants. Transfection with WT WIPI2 or WIPI2-FKKG, but not WIPI2-FTTG or WIPI2-R108E/R125E (2RE), attenuated the Ara-C-stimulated increase in the level of *Ifnb1* mRNA (Fig 6D). In addition, we examined the *Ifnb1* mRNA level in *Sting*-KO cells after re-introduction of WT STING or STING mutants, including STING-L333A/R334A, which cannot be exported from the ER, and STING-R238A, which cannot bind to cGAMP (Gui *et al*, 2019). Transfection with WT STING, but not STING-L333A/R334A or the STING-R238A, increased the level of *Ifnb1* mRNA in the cells (Fig 6E). Transfection with STING-3A-2, which cannot bind to WIPI2, further enhanced *Ifnb1* expression (Fig 6E). Finally, after re-introduction of WT STING or STING-3A-2, we conducted a time-course experiment by examining cGAS-STING signaling in *Sting*-KO cells. Obviously, after cGAMP stimulation, the protein level of WT STING but not STING-3A-2 decreased significantly (Fig 6F). Compared with WT STING-expressing cells, the phosphorylation of TBK1, IRF3, and STING decreased less in STING-3A-2-expressing cells after long-term (12 h) cGAMP treatment (Fig 6F and G). Consistent with this, cells expressing STING-3A-2 showed much higher *Ifnb1* mRNA levels after long-term (12 h) cGAMP treatment (Fig 6H). Taken together, these results suggest that STING-WIPI2 interaction is required for the attenuation of activated cGAS-STING signaling.

Discussion

In this study, we have revealed a STING-dependent mechanism for membrane recruitment of WIPI2 during autophagy initiated by the cGAS-STING pathway. This mechanism requires the direct interaction between STING and WIPI2. Our results prove the necessity for WIPI2 and suggest that STING and PI3P compete for WIPI2. There is a mutual functional inhibition between PI3P-dependent canonical autophagy and PI3P-independent noncanonical autophagy (Fig 7).

Accumulating evidence has confirmed the indispensable role of WIPI2 in autophagosome formation triggered by different cues (Polson *et al*, 2010; Dooley *et al*, 2014; Thurston *et al*, 2016; Zhao *et al*, 2017; Wan *et al*, 2018; Gui *et al*, 2019; Fracchiolla *et al*, 2020). However, most of our understanding of WIPI2 recruitment to phagphores comes from starvation-induced canonical autophagy, in which WIPI2 is directed to the formed phagophores through interaction with PI3P on the membranes. Here, we show that WIPI2 can bind to inactivated or activated STING, and the binding is essential for STING-induced LC3 lipidation and autophagosome formation. These results suggest that, unlike canonical PI3P-dependent autophagy, in STING-induced autophagosome formation, WIPI2 is already localized to the membranes during phagophore biogenesis. This may explain the dispensability of PI3P and the importance of STING trafficking in STING-induced autophagy. Besides cytoplasmic DNA, which activates cGAS-STING signaling, PI3P-independent autophagosome formation can also be triggered by other stimuli such as unsaturated fatty acids (Niso-Santano *et al*, 2015). It will be interesting to investigate whether WIPI2 is similarly recruited to the phagophores through binding to STING or other transmembrane proteins.

Through the identification of the STING-binding motif in WIPI2, we have elucidated that STING and PI3P compete for WIPI2. Our results demonstrate that the inhibition of PIK3C3 complex can promote STING-induced autophagy by facilitating STING-WIPI2 interaction, while deletion of *STING* can augment basal and starvation-induced canonical autophagy. However, the inhibition of PIK3C3 complex did not affect the activation of STING, because it influenced neither the formation of STING vesicles nor the phosphorylation of TBK1 in cGAMP-treated cells. This supports the view that PIK3C3 complex-mediated PI3P synthesis is unnecessary in the cGAS-STING pathway for the activation of TBK1 and IRF3 (Gui *et al*, 2019; Liu *et al*, 2019), but it is inconsistent with the observation that PI3P is required for the ER exit of STING (Zhang *et al*, 2020), an essential and rate-limiting step of the cGAS-STING pathway. Although the PI3P-dependent and PI3P-independent mechanisms for STING trafficking need further investigation, we show that unlike the other known STING-interacting proteins (Luo *et al*, 2016; Sun *et al*, 2018; Yang *et al*, 2018), the binding of WIPI2 to STING does not affect STING activation and its intracellular trafficking. This suggests that the direct effect of STING-WIPI2 interaction

---

Figure 6. Role of STING-WIPI2 interaction in attenuating activated cGAS-STING signaling.

A   *Wipi2*- or *Sting*-deleted MEFs were treated with Ara-C for 12 h and then cultured in Ara-C-free medium. After 24 h, the cells were lysed and analyzed by western blot using the indicated antibodies.

B   Statistical analysis of the protein level of phospho-TBK1 (Ser172) and STING in cells treated as in (A). The relative phospho-TBK1 level was normalized to TBK1, and the relative STING level was normalized to Actin.

C–E   MEFs with *Wipi2* or *Sting* deletion (C), *Wipi2*-KO MEFs with transfection of Myc-tagged WT or mutant WIPI2 (D), or *Sting*-KO MEFs with transfection of HA-tagged WT or mutant STING (E), were treated with Ara-C for 12 h and then cultured in Ara-C-free medium for another 24 h. Total mRNA was extracted and the *Ifnb1* mRNA level was measured by real-time PCR and normalized to *Actb* mRNA. 2RE, WIPI2-R108E/R125E.

F   *Sting*-KO MEFs with transfection of HA-tagged WT or mutant STING were treated with cGAMP for the indicated time. The cells were lysed and analyzed by western blot using the indicated antibodies.

G   Statistical analysis of the protein level of phospho-IRF3 (Ser396), phospho-TBK1 (Ser172), and phospho-STING (Ser366) in cells treated as in (F). The relative level of these phosphorylated proteins was normalized to IRF3, TBK1, and STING, respectively.

H   Statistical analysis of the *Ifnb1* mRNA level in cells treated as in (F). The relative *Ifnb1* mRNA level was normalized to *Actb* mRNA.

Data information: All statistical data are presented as mean ± SEM of three independent experiments. **$P < 0.01$, ***$P < 0.001$ (Student's *t*-test).
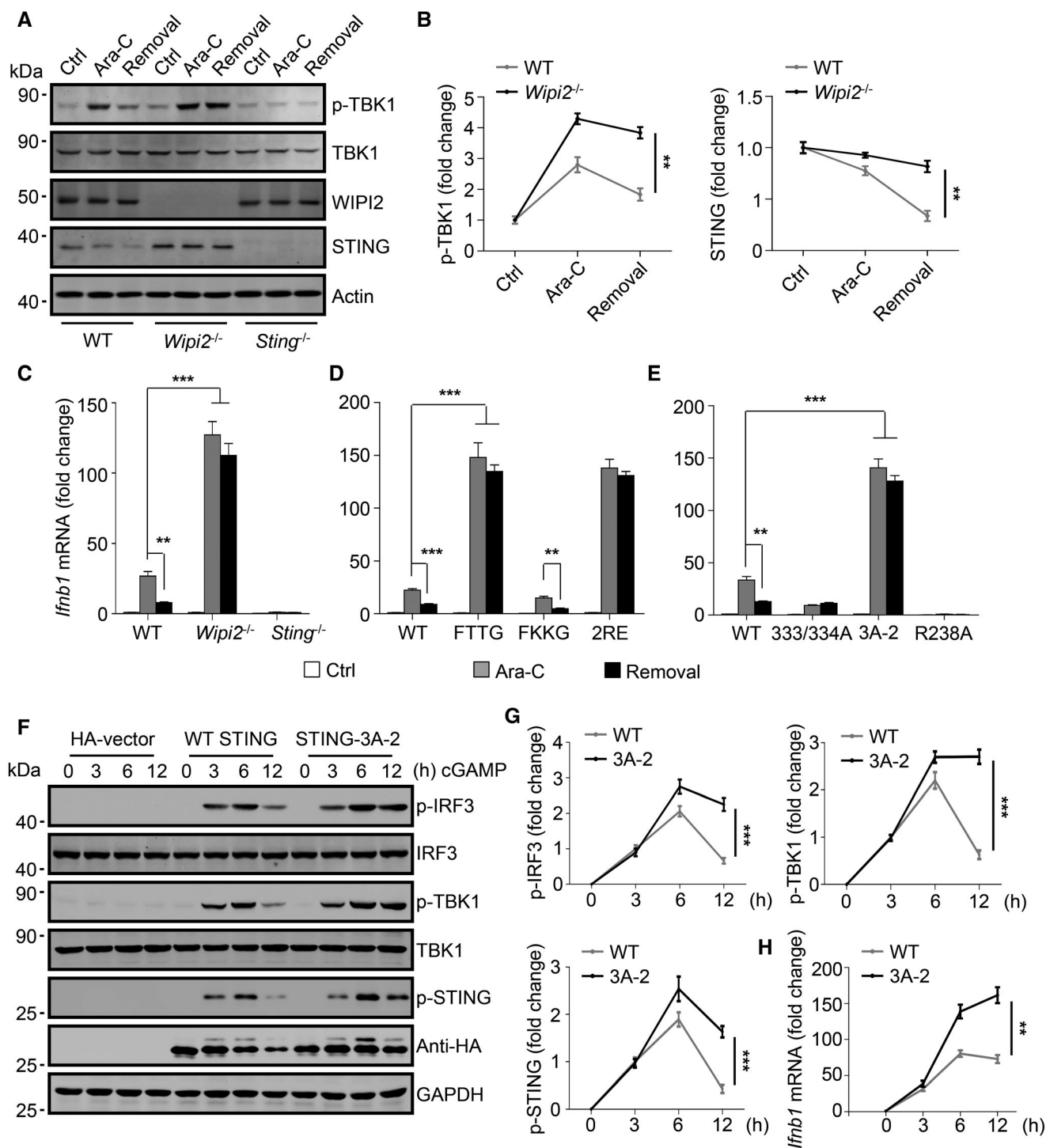Source data are available online for this figure.

Figure 6.

is limited to STING-induced autophagy but not type I IFN production. Nevertheless, our results suggest that WIPI2 is critical in coordinating PI3P-dependent canonical autophagy and PI3P-independent noncanonical autophagy. Given the key role of STING-induced autophagy in combating pathogens and preventing excessive inflammation (Liang et al, 2014; Prabakaran et al, 2018; Gui et al, 2019), targeting WIPI2 expression and PIK3C3 complex 1 activity might be

a promising strategy for the treatment of viral/bacterial infections and autoimmune diseases.

Recently, it was suggested that ATG16L1 can be recruited to peri-nuclear single-membrane STING vesicles for LC3 lipidation, depending on the interaction between the WD40 domain of ATG16L1 and V-ATPase in the membranes (Fischer et al, 2020). Here, we show that targeting ATG16L1 to the phagophore-forming
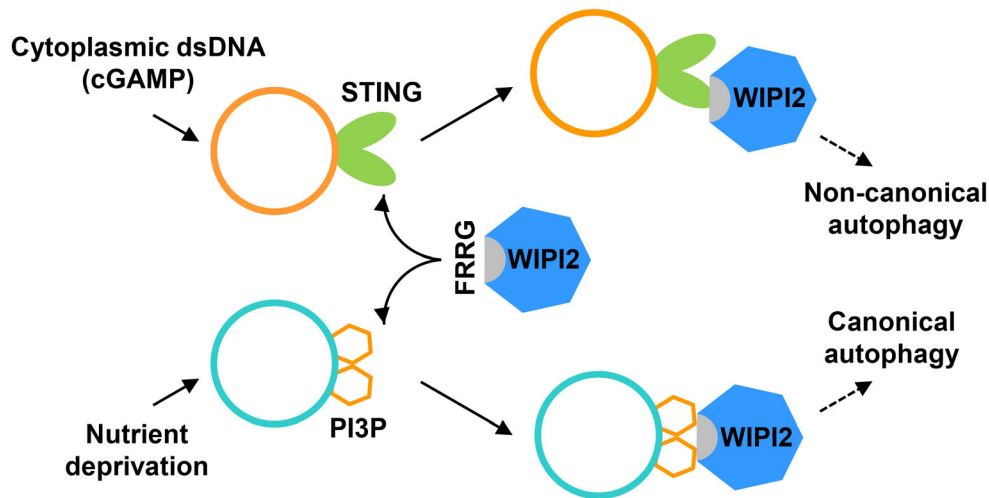
Figure 7. Schematic model for the membrane recruitment of WIPI2.

The binding of WIPI2 to the phagophore is essential for LC3 lipidation and autophagosome formation. WIPI2 is recruited by membrane PI3P in starvation-induced autophagy, whereas it is recruited by membrane STING in cGAS-STING pathway-mediated autophagy. The competition between PI3P and STING for binding to WIPI2 leads to mutual inhibition between PI3P-dependent canonical autophagy and PI3P-independent noncanonical autophagy.

STING vesicles is independent of its WD40 domain. This difference could be explained by the absence or presence of WIPI2 on these membranes. In phagophore-forming STING vesicles, ATG16L1 could be recruited through binding to WIPI2, but on perinuclear single-membrane STING vesicles, ATG16L1 needs its WD40 domain to interact with V-ATPase due to the lack of WIPI2.

Increasing evidence shows that the expression of STING is silent in many cancer cells (Xia *et al*, 2016a,b). This may allow more WIPI2 to bind to PI3P, thereby increasing the level of basal autophagy in these cells. The high level of autophagy in cancer cells is an important cause of chemotherapy and radiotherapy resistance. Further study is warranted to determine whether the binding of WIPI2 to PI3P promotes the upregulation of autophagy in STING-deficient cancer cells.

Materials and Methods

Plasmids and oligonucleotides

WIPI2-Myc, WIPI1-Myc, GST-WIPI2, WIPI2a-GFP, WIPI2b-GFP, WIPI2c-GFP, WIPI2d-GFP, GFP-STX17, and GFP-LC3 were described previously (Wan *et al*, 2017, 2018; Shen *et al*, 2021). GFP-tagged WIPI2a, WIPI2b, WIPI2c, and WIPI2d were different human WIPI2 isoforms, WIPI2 or WIPI2 mutants harbored in all other constructs were mouse WIPI2, which has only one isoform. GFP-DFCP1 and STING (human)-HA were gifts from Dr. Hong Zhang (Institute of Biophysics, Chinese Academy of Sciences, China) and Dr. Quan Chen (Nankai University, China), respectively. WIPI2-GFP and ATG14L-GFP were constructed by inserting the corresponding cDNA into a pEGFP-N1 vector, and HA-DFCP1 was constructed by inserting the cDNA into a pRK5-HA vector. Site-directed mutagenesis was performed using QuikChange II XL (Stratagene) according to the manufacturer's instructions. Truncated mutants were constructed by inserting the corresponding cDNA fragments into the vector. The following Cy3-ISD sequences were used (Du & Chen, 2018), sense,

Cy3-TACAGATCTACTAGTGATCTATGACTGATCTGTACATGATCT ACA, anti-sense, TGTAGATCATGTACAGATCAGTCATAGATCACTA GTAGATCTGTA. For RNA interference, the following siRNA duplexes were used, control siRNA, AAGACCAAUUUCAGCAGACAGTT, WIPI2 siRNA, GACAGUCCUUUAGCGGCATT. For real-time PCR analysis, the following primers were used: human *IFNB1* forward, CATTACCTG AAGGCCAAGGA; human *IFNB1* reverse, CAATTGTCCAGTCCCAG AGG; human *GAPDH* forward, ACAGTCAGCCGCATCTTCTT; human *GAPDH* reverse, ACGACCAAATCCGTTGACTC; mouse *Ifnb1* forward, AGGGCGGACTTCAAGATC; mouse *Ifnb1* reverse, CTCATTCC ACCCAGTGCT; mouse *Actb* forward, GGCTGTATTCCCCTCCATCG; mouse *Actb* reverse, CCAGTTGGTAACAATGCCATGT.

Antibodies

The following primary antibodies were used, anti-dsDNA (mouse, Abcam, ab27156), anti-LAMP2 (rabbit, Abcam, ab199946), anti-WIPI1 (rabbit, Abcam, ab128901), anti-WIPI2 (mouse, Abcam, ab105459), anti-GM130 (rabbit, Cell Signaling Technology, 12480S), anti-phospho-IRF3 (Ser396; rabbit, Cell Signaling Technology, 4947S), anti-IRF3 (rabbit, Cell Signaling Technology, 4302S), anti-NBR1 (rabbit, Cell Signaling Technology, 9891S), anti-phospho-STING (Ser366; rabbit, Cell Signaling Technology, 19781S), anti-STING (rodent preferred; rabbit, Cell Signaling Technology, 50494S), anti-phospho-TBK1/NAK (Ser172; rabbit, Cell Signaling Technology, 5483S), anti-TBK1/NAK (rabbit, Cell Signaling Technology, 3504S), anti-WIPI2 (rabbit, Cell Signaling Technology, 8567), anti-LC3 (mouse, Cosmo Bio, CAC-CTB-LC3-2-IC), anti-ATG16L1 (rabbit, MBL, PM040), anti-HA (mouse, MBL, M180-3), anti-HA (rabbit, MBL, 561), anti-LC3 (rabbit, MBL, PM036), anti-Myc (mouse, MBL, M192-3), anti-Myc (rabbit, MBL, 562), anti-ATG5 (rabbit, Novus Biologicals, NB110-53818), anti-TFR (rabbit, Novus Biologicals, NB100-92243), anti-BECN1 (rabbit, Proteintech, 11306-1-AP), anti-CALR (rabbit, Proteintech, 27298-1-AP), anti-GAPDH (rabbit, Proteintech, 10494-1-AP), anti-p62/SQSTM1 (rabbit, Proteintech,

18420-1-AP), anti-STING (for endogenous STING staining; rabbit, Proteintech, 19851-1-AP), anti-GFP (mouse, Santa Cruz Biotechnology, sc-9996), anti-GST (rabbit, Santa Cruz Biotechnology, sc-459), anti-β-Actin (mouse, Sigma-Aldrich, A5316), anti-β-Tubulin (mouse, Sigma-Aldrich, T8328), anti-ERGIC-53/p58 (rabbit, Sigma-Aldrich, E1031), anti-LC3B (rabbit, Sigma-Aldrich, L7543), and anti-WIPI2 (rabbit, Sigma-Aldrich, SAB4200399). The following secondary antibodies were used for western blot, donkey anti-rabbit IgG (H + L) IRDye800CW (LI-COR Biosciences, 926-32213), donkey anti-mouse IgG (H + L) IRDye680RD (LI-COR Biosciences, 926-68072). The following secondary antibodies were used for immunostaining, goat anti-mouse IgG (H + L), Alexa Fluor 488 (Thermo Fisher Scientific, A-11001), donkey anti-rabbit IgG (H + L), Alexa Fluor 488 (Thermo Fisher Scientific, A-21206), donkey anti-mouse IgG (H + L), Alexa Fluor 546 (Thermo Fisher Scientific, A10036), donkey anti-rabbit IgG (H + L), Alexa Fluor 546 (Thermo Fisher Scientific, A10040), goat anti-mouse IgG (H + L), Alexa Fluor 635 (Thermo Fisher Scientific, A-31574), goat anti-rabbit IgG (H + L), Alexa Fluor 635 (Thermo Fisher Scientific, A-31576). Anti-HA magnetic beads (Bimake, B26202) and anti-Myc magnetic beads (Bimake, B26302) were used for immunoprecipitation assay, glutathione-sepharose 4B beads (GE Healthcare Life Sciences, 17-0756-01) were used for GST pull-down assay.

Cell culture and transfection

HEK293T, HEK293, DLD1, or MEFs were cultured in DMEM supplemented with 10% FBS. *BECN1* knockout HEK293 cells and *Atg5* knockout MEFs were described previously (Huang *et al*, 2015; Su *et al*, 2017). *Wipi2* knockout MEFs, *Sting* knockout MEFs, and *TBK1* knockout DLD1 cells were from Dr. Hong Zhang (Institute of Biophysics, Chinese Academy of Sciences, China), Dr. Quan Chen (Nankai University, China) and Dr. Pinglong Xu (Zhejiang University, China), respectively. Cell lines were recently authenticated by STR profiling and tested for mycoplasma contamination. To obtain human monocyte-derived macrophages, peripheral blood mononuclear cells (PBMCs) were isolated from the peripheral blood of healthy volunteers (Solarbio, P8670). Institutional review board approval and ethics committee approval were granted, and the informed consent was obtained from all volunteers. The collection of the peripheral blood and the isolation of PBMCs were according to the blind strategy. Monocytes from the PBMCs were separated by adherence to plastic in RPMI 1640 supplemented with 10% human serum. Differentiation of monocytes to macrophages was achieved by culturing in DMEM supplemented with 10% heat-inactivated human serum for 10 days in the presence of 10 ng/ml M-CSF (R&D Systems, 216MC025CF). Lipofectamine 3000 (Invitrogen, L3000015) was used for plasmids transient transfection according to the manufacturer's instructions. Stable cell lines were generated by transient transfection followed by selection with G418 or puromycin. For siRNA knockdown in primary human cells (Prabakaran *et al*, 2018), cells were transfected with WIPI2 siRNAs or control siRNAs using Lipofectamine 3000 on days 6 and 8 into the differentiation procedure. The human monocyte-derived macrophages were used for experiments after 10 days of differentiation.

Reagents and treatment

The chemicals were used as follows unless indicated otherwise: cGAMP (InvivoGen, tlrl-nacga23-1), 500 nM; Brefeldin A (BFA;

Selleckchem, S7046), 5 μM; BX795 (Selleckchem, S1274), 10 μM; Torin1 (Selleckchem, S2827), 50 nM; chloroquine (CQ; Sigma-Aldrich, C6628), 10 μM; MG132 (Sigma-Aldrich, SML1135), 5 μM; VPS34-IN1 (Selleckchem, S7980), 5 μM; arabinofuranosyl cytidine (Ara-C; Selleckchem, S1648), 5 μM. cGAMP was delivered into cells by permeabilization with digitonin (10 μg/ml) for 15 min in buffer A (50 mM HEPES-KOH, pH 7.2, 100 mM KCl, 3 mM $MgCl_2$, 0.1 mM DTT, 85 mM sucrose, 0.2% BSA, 1 mM ATP). Cy3-ISD was transfected into cells using Lipofectamine 3000. Cells were incubated with EBSS referred to as starvation.

Immunostaining and cell imaging

For immunostaining, HEK293T, DLD1 cells or MEFs were fixed with 4% formaldehyde in PBS for 15 min at room temperature and permeabilized with 0.1% saponin in PBS for 10 min. Then, the cells were incubated with appropriate primary and secondary antibodies in 0.1% saponin as indicated. For immunostaining of cytoplasmic DNA (Spada *et al*, 2019), to allow the antibody to cross the cellular but not the nuclear membrane, DLD1 cells or MEFs were permeabilized with permeabilization buffer (0.1% Tween 20, 0.01% Triton X-100 in PBS) for 7 min at room temperature. After immunostaining, the cell nuclei were stained with DAPI Fluoromount-G (Southern Biotech, 0100-20).

Confocal images were captured in multitracking mode on a laser scanning confocal microscope with a 63 × plan apochromat 1.4 NA objective on the Zeiss LSM880. In some experiments, images were processed using ImageJ. 3D z-stack reconstruction was generated using Imaris.

Immunoprecipitation and western blot

For immunoprecipitation, cells were lysed in Nonidet P40 (NP-40) buffer (50 mM Tris–HCl, pH 7.4, 1% NP-40, 150 mM NaCl, 2 mM EDTA, 1 mM DTT, 10% glycerol) supplemented with protease inhibitors and phosphatase inhibitors and mixed with anti-HA or anti-Myc affinity beads at 4°C overnight. The immunocomplexes were washed extensively four times and resolved in an SDS sample buffer. To examine the effects of lipids on STING-WIPI2 interaction, the immunocomplexes were washed with NP-40 buffer and resuspended in liposome binding buffer (150 mM NaCl, 50 mM Tris–HCl, pH 7.5, 1 mM DTT) supplemented with protease inhibitors and phosphatase inhibitors (Dudley *et al*, 2019). After incubation with PI3P- or PI-decorated liposomes (Echelon, Y-P000-3, or Y-P003-3) at 4°C for 2 h, immunocomplexes were washed and resolved in SDS sample buffer. Western blot was performed as described previously (Xu *et al*, 2016). In brief, samples were separated with SDS–PAGE, transferred to polyvinylidene difluoride (PVDF) membrane, and probed with the corresponding antibodies. The specific bands were analyzed using an Odyssey Infrared Imaging System.

Protein expression and purification

GST-tagged WIPI2 and WIPI2 mutants, STING-153-379, and STING-153-379 mutants were expressed in *Escherichia coli* BL21 (Transgen Biotech, CD601) by induction with 0.1 mM isopropyl β-D-thiogalactopyranoside (Sigma-Aldrich, I5502) for 12 h at 28°C. The recombinant proteins were purified using glutathione-sepharose

4B beads, and eluted with glutathione or incubated with thrombin at 4°C for 6 h to release the proteins from the GST.

In vitro GST pull-down assay

Purified GST, STING-153-379, and STING-153-379-3A-2 proteins were incubated with purified WIPI2, WIPI2-FTTG, or WIPI2-FKKG proteins, respectively. After incubation for 4 h at 4°C, glutathione-sepharose 4B beads were added to the mixture, followed by further incubation for 2 h at 4°C. The beads were washed with NP-40 buffer for four times. The beads-bound proteins were analyzed by western blot.

STING vesicles isolation

HEK293T cells stably expressing STING-HA were stimulated with cGAMP and harvested, washed, and homogenized in extraction buffer (5 mM MOPS, pH 7.65, 0.25 M sucrose, 1 mM EDTA, 0.1% ethanol, and protease inhibitors and phosphatase inhibitors). The lysates were mixed with anti-HA affinity beads at 4°C for 4 h. The bound STING vesicles were washed using an extraction buffer for four times and subjected to the mass spectrometry analysis or the protease protection assay.

Immunoisolation

Immunoisolation of HA-DFCP1-positive membranes was described previously with some modifications (Judith *et al*, 2019). Briefly, cells stably expressing HA-DFCP1 were treated with EBSS or Torin1 and harvested, washed, and homogenized in isotonic buffer (20 mM HEPES, pH 7.4, 250 mM sucrose, and 1 mM EDTA, protease inhibitors, and phosphatase inhibitors). The lysates were then subjected to centrifugation at 3,000 *g* at 4°C and the supernatants were incubated with anti-HA affinity beads at 4°C for 4 h. The HA-DFCP1-positive membranes on the beads were washed four times with isotonic buffer supplemented with 150 mM NaCl and subjected to western blot.

Membrane fractionation

Membrane fractionation was performed as described previously (Ge *et al*, 2013; Gui *et al*, 2019). Briefly, cells (30 10-cm dishes) were treated with or without cGAMP, then collected and homogenized. Homogenates were then subjected to sequential centrifugation at 1,000 *g* (10 min), 5,000 *g* (10 min), and 25,000 *g* (20 min) to collect the P1, P5, and P25 membranes, respectively. The P25 membranes were suspended in 0.75 ml 1.25 M sucrose buffer and overlayed with 0.5 ml 1.1 M and 0.5 ml 0.25 M sucrose buffer. Centrifugation was carried out at 120,000 *g* for 3 h. The P25L fraction at the interface between the 0.25 M and 1.1 M sucrose layers was selected and suspended in 1 ml 19% Opti-Prep for the following Opti-Prep step gradient from bottom to top: 0.33 ml 22.5%, 0.66 ml 19% (sample), 0.6 ml 16%, 0.6 ml 12%, 0.66 ml 8%, 0.33 ml 5%, and 0.14 ml 0%. Each density of Opti-Prep was prepared by diluting 50% Opti-Prep (20 mM Tricine-KOH, pH 7.4, 42 mM sucrose, and 1 mM EDTA) with a buffer of 20 mM Tricine-KOH, pH 7.4, 250 mM sucrose, and 1 mM EDTA. The Opti-Prep gradient was centrifuged at 150,000 *g* for 3 h and 10 fractions, 0.5 ml each, were collected from the top. Fractions were diluted and subjected to immunoprecipitation.

Protease protection assay

STING-HA-positive vesicles were incubated with trypsin and/or 0.5% Triton X-100 for 90 min at 37°C. Reactions were terminated by the addition of the SDS sample buffer. The samples were then subjected to western blot.

cGAMP measurement

Cells were harvested by trypsinization. Cell pellets were lysed and centrifuged for 5 min at 15,000 *g* at 4°C. Relative cGAMP measurements of the supernatants were carried out using a 2′-3′-cGAMP ELISA kit (Cayman, 501700) according to the manufacturer's instructions. Protein concentration in the supernatant was measured using BCA Pierce Protein assay kit and was used to normalize cGAMP concentration.

RNA extraction and real-time PCR

Total RNA was isolated from cells using TRIzol (Thermo Fisher Scientific, 15596018). Reverse transcription was performed using M-MLV reverse transcription reagents (Promega). The resulting cDNA was subjected to real-time PCR analysis with gene-specific primers in the presence of SYBR Green PCR Master Mix (Takara) using the ABI7500 real-time PCR system.

HPLC-MS/MS

Mass spectrometry analysis of samples was described previously (Wan *et al*, 2018). To identify proteins that target to STING vesicles, HEK293T cells stably expressing STING-HA were stimulated with cGAMP. STING vesicles were isolated with anti-HA affinity beads and washed four times, and then dissolved with 40 μl urea (8 M)/DTT (10 mM). The mixture was sonicated for 30 min at room temperature and then sequentially treated with IAA (10 mM) and trypsin to alkylate the resulting thiol group and digest the proteins for 16 h at 37°C at an enzyme-to-substrate ratio of 1:50 (w/w). The tryptic digested peptides were then subjected to HPLC-MS/MS analysis.

Statistical analysis

All the statistical data are presented as mean ± SEM. The statistical significance of differences was determined using Student's *t*-test. $P < 0.05$ was considered to be statistically significant.

Data availability

This study includes no data deposited in external repositories.

Expanded View for this article is available online.

Author contributions

Wei Wan: Conceptualization; resources; data curation; software; formal analysis; supervision; funding acquisition; investigation; methodology; writing – original draft; project administration; writing – review and editing. **Chuying Qian:** Resources; formal analysis; investigation. **Qian Wang:** Resources; formal analysis; investigation. **Jin Li:** Resources; methodology. **Hongtao Zhang:** Resources; methodology. **Lei Wang:** Resources; formal analysis; investigation; methodology. **Maomao Pu:** Resources; methodology. **Yewei Huang:** Resources; methodology. **Zhengfu He:** Resources; methodology. **Tianhua Zhou:** Resources; formal analysis. **Han-Ming Shen:** Resources; formal analysis. **Wei Liu:** Conceptualization; supervision; funding acquisition; writing – original draft; project administration; writing – review and editing.

Disclosure and competing interests statement

The authors declare that they have no conflict of interest.

References

Bago R, Malik N, Munson MJ, Prescott AR, Davies P, Sommer E, Shpiro N, Ward R, Cross D, Ganley IG *et al* (2014) Characterization of VPS34-IN1, a selective inhibitor of Vps34, reveals that the phosphatidylinositol 3-phosphate-binding SGK3 protein kinase is a downstream target of class III phosphoinositide 3-kinase. *Biochem J* 463: 413–427

Chen MX, Meng QC, Qin YF, Liang PP, Tan P, He L, Zhou YB, Chen YJ, Huang JJ, Wang RF *et al* (2016a) TRIM14 inhibits cGAS degradation mediated by selective autophagy receptor p62 to promote innate immune responses. *Mol Cell* 64: 105–119

Chen Q, Sun L, Chen ZJ (2016b) Regulation and function of the cGAS-STING pathway of cytoplasmic DNA sensing. *Nat Immunol* 17: 1142–1149

Chu TT, Tu XT, Yang K, Wu JJ, Repa JJ, Yan N (2021) Tonic prime-boost of STING signalling mediates Niemann-pick disease type C. *Nature* 596: 570–575

Davis S, Wang J, Zhu M, Stahmer K, Lakshminarayan R, Ghassemian M, Jiang Y, Miller EA, Ferro-Novick S (2016) Sec24 phosphorylation regulates autophagosome abundance during nutrient deprivation. *Elife* 5: e21167

Dooley HC, Razi M, Polson HE, Girardin SE, Wilson MI, Tooze SA (2014) WIPI2 links LC3 conjugation with PI3P, autophagosome formation, and pathogen clearance by recruiting Atg12-5-16L1. *Mol Cell* 55: 238–252

Du MJ, Chen ZJJ (2018) DNA-induced liquid phase condensation of cGAS activates innate immune signaling. *Science* 361: 704–709

Dudley LJ, Cabodevilla AG, Makar AN, Sztacho M, Michelberger T, Marsh JA, Houston DR, Martens S, Jiang XJ, Gammoh N (2019) Intrinsic lipid binding activity of ATG16L1 supports efficient membrane anchoring and autophagy. *EMBO J* 38: e100554

Fischer TD, Wang C, Padman BS, Lazarou M, Youle RJ (2020) STING induces LC3B lipidation onto single-membrane vesicles via the V-ATPase and ATG16L1-WD40 domain. *J Cell Biol* 219: e202009128

Fletcher K, Ulferts R, Jacquin E, Veith T, Gammoh N, Arasteh JM, Mayer U, Carding SR, Wileman T, Beale R *et al* (2018) The WD40 domain of ATG16L1 is required for its non-canonical role in lipidation of LC3 at single membranes. *EMBO J* 37: e97840

Fracchiolla D, Chang C, Hurley JH, Martens S (2020) A PI3K-WIPI2 positive feedback loop allosterically activates LC3 lipidation in autophagy. *J Cell Biol* 219: e201912098

Ge L, Melville D, Zhang M, Schekman R (2013) The ER-Golgi intermediate compartment is a key membrane source for the LC3 lipidation step of autophagosome biogenesis. *Elife* 2: e00947

Ge L, Zhang M, Schekman R (2014) Phosphatidylinositol 3-kinase and COPII generate LC3 lipidation vesicles from the ER-Golgi intermediate compartment. *Elife* 3: e04135

Grant S (1998) Ara-C: cellular and molecular pharmacology. *Adv Cancer Res* 72: 197–233

Gui X, Yang H, Li T, Tan XJ, Shi PQ, Li MH, Du FH, Chen ZJJ (2019) Autophagy induction via STING trafficking is a primordial function of the cGAS pathway. *Nature* 567: 262–266

Huang R, Xu Y, Wan W, Shou X, Qian J, You Z, Liu B, Chang C, Zhou T, Lippincott-Schwartz J *et al* (2015) Deacetylation of nuclear LC3 drives autophagy initiation under starvation. *Mol Cell* 57: 456–466

Ishikawa H, Ma Z, Barber GN (2009) STING regulates intracellular DNA-mediated, type I interferon-dependent innate immunity. *Nature* 461: 788–792

Itakura E, Kishi-Itakura C, Mizushima N (2012) The hairpin-type tail-anchored SNARE syntaxin 17 targets to autophagosomes for fusion with endosomes/lysosomes. *Cell* 151: 1256–1269

Jena KK, Mehto S, Nath P, Chauhan NR, Sahu R, Dhar K, Das SK, Kolapalli SP, Murmu KC, Jain A *et al* (2020) Autoimmunity gene IRGM suppresses cGAS-STING and RIG-I-MAVS signaling to control interferon response. *EMBO Rep* 21: e50051

Jiang LQ, Xia T, Hu YH, Sun MS, Yan S, Lei CQ, Shu HB, Guo JH, Liu Y (2018) IFITM3 inhibits virus-triggered induction of type I interferon by mediating autophagosome-dependent degradation of IRF3. *Cell Mol Immunol* 15: 858–867

Judith D, Jefferies HBJ, Boeing S, Frith D, Snijders AP, Tooze SA (2019) ATG9A shapes the forming autophagosome through arfaptin 2 and phosphatidylinositol 4-kinase III beta. *J Cell Biol* 218: 1634–1652

Li XD, Wu J, Gao D, Wang H, Sun L, Chen ZJ (2013) Pivotal roles of cGAS-cGAMP signaling in antiviral defense and immune adjuvant effects. *Science* 341: 1390–1394

Liang QM, Seo GJ, Choi YJ, Kwak MJ, Ge JN, Rodgers MA, Shi MD, Leslie BJ, Hopfner KP, Ha T *et al* (2014) Crosstalk between the cGAS DNA sensor and beclin-1 autophagy protein shapes innate antimicrobial immune responses. *Cell Host Microbe* 15: 228–238

Liu D, Wu H, Wang C, Li Y, Tian H, Siraj S, Sehgal SA, Wang X, Wang J, Shang Y *et al* (2019) STING directly activates autophagy to tune the innate immune response. *Cell Death Differ* 26: 1735–1749

Lu Q, Yang PG, Huang XX, Hu WQ, Guo B, Wu F, Lin L, Kovacs AL, Yu L, Zhang H (2011) The WD40 repeat PtdIns(3)P-binding protein EPG-6 regulates progression of omegasomes to autophagosomes. *Dev Cell* 21: 343–357

Lu G, Yi J, Gubas A, Wang YT, Wu YH, Ren Y, Wu M, Shi Y, Ouyang CX, Tan HWS *et al* (2019) Suppression of autophagy during mitosis via CUL4-RING ubiquitin ligases-mediated WIPI2 polyubiquitination and proteasomal degradation. *Autophagy* 15: 1917–1934

Luo WW, Li S, Li C, Lian H, Yang Q, Zhong B, Shu HB (2016) iRhom2 is essential for innate immunity to DNA viruses by mediating trafficking and stability of the adaptor STING. *Nat Immunol* 17: 1057–1066

Ma RH, Serrano TPO, Davis J, Prigge AD, Ridge KM (2020) The cGAS-STING pathway: the role of self-DNA sensing in inflammatory lung disease. *FASEB J* 34: 13156–13170

McNab F, Mayer-Barber K, Sher A, Wack A, O'Garra A (2015) Type I interferons in infectious disease. *Nat Rev Immunol* 15: 87–103

Motwani M, Pesiridis S, Fitzgerald KA (2019) DNA sensing by the cGAS-STING pathway in health and disease. *Nat Rev Genet* 20: 657–674

Niso-Santano M, Malik SA, Pietrocola F, Bravo-San Pedro JM, Marino G, Cianfanelli V, Ben-Younes A, Troncoso R, Markaki M, Sica V *et al* (2015) Unsaturated fatty acids induce non-canonical autophagy. *EMBO J* 34: 1025–1041

Ohnstad AE, Delgado JM, North BJ, Nasa I, Kettenbach AN, Schultz SW, Shoemaker CJ (2020) Receptor-mediated clustering of FIP200 bypasses the role of LC3 lipidation in autophagy. *EMBO J* 39: e104948

Polson HE, de Lartigue J, Rigden DJ, Reedijk M, Urbe S, Clague MJ, Tooze SA (2010) Mammalian Atg18 (WIPI2) localizes to omegasome-anchored phagophores and positively regulates LC3 lipidation. *Autophagy* 6: 506–522

Prabakaran T, Bodda C, Krapp C, Zhang BC, Christensen MH, Sun CL, Reinert L, Cai YJ, Jensen SB, Skouboe MK *et al* (2018) Attenuation of cGAS-STING signaling is mediated by a p62/SQSTM1-dependent autophagy pathway activated by TBK1. *EMBO J* 37: e97858

Ramanjulu JM, Pesiridis GS, Yang J, Concha N, Singhaus R, Zhang SY, Tran JL, Moore P, Lehmann S, Eberl HC *et al* (2018) Design of amidobenzimidazole STING receptor agonists with systemic activity. *Nature* 564: 439–443

Shen QH, Shi Y, Liu JQ, Su H, Huang JT, Zhang Y, Peng C, Zhou TH, Sun QM, Wan W *et al* (2021) Acetylation of STX17 (syntaxin 17) controls autophagosome maturation. *Autophagy* 17: 1157–1169

Spada S, Yamazaki T, Vanpouille-Box C (2019) Detection and quantification of cytoplasmic DNA. *Methods Enzymol* 629: 17–33

Su H, Yang F, Wang QT, Shen QH, Huang JT, Peng C, Zhang Y, Wan W, Wong CCL, Sun QM *et al* (2017) VPS34 acetylation controls its lipid kinase activity and the initiation of canonical and non-canonical autophagy. *Mol Cell* 67: 907–921

Sui HY, Zhou M, Imamichi H, Jiao XL, Sherman BT, Lane HC, Imamichi T (2017) STING is an essential mediator of the Ku70-mediated production of IFN-gimel 1 in response to exogenous DNA. *Sci Signal* 10: eaah5054

Sun MS, Zhang J, Jiang LQ, Pan YX, Tan JY, Yu F, Guo L, Yin L, Shen C, Shu HB *et al* (2018) TMED2 potentiates cellular IFN responses to DNA viruses by reinforcing MITA dimerization and facilitating its trafficking. *Cell Rep* 25: 3086–3098

Thurston TL, Boyle KB, Allen M, Ravenhill BJ, Karpiyevich M, Bloor S, Kaul A, Noad J, Foeglein A, Matthews SA *et al* (2016) Recruitment of TBK1 to cytosol-invading salmonella induces WIPI2-dependent antibacterial autophagy. *EMBO J* 35: 1779–1792

Valverde DP, Yu SL, Boggavarapu V, Kumar N, Lees JA, Walz T, Reinisch KM, Melia TJ (2019) ATG2 transports lipids to promote autophagosome biogenesis. *J Cell Biol* 218: 1787–1798

Wan W, You Z, Xu Y, Zhou L, Guan Z, Peng C, Wong CCL, Su H, Zhou T, Xia H *et al* (2017) mTORC1 phosphorylates acetyltransferase p300 to regulate autophagy and lipogenesis. *Mol Cell* 68: 323–335

Wan W, You Z, Zhou L, Xu Y, Peng C, Zhou T, Yi C, Shi Y, Liu W (2018) mTORC1-regulated and HUWE1-mediated WIPI2 degradation controls autophagy flux. *Mol Cell* 72: 303–315

Watson RO, Manzanillo PS, Cox JS (2012) Extracellular *M. tuberculosis* DNA targets bacteria for autophagy by activating the host DNA-sensing pathway. *Cell* 150: 803–815

Watson RO, Bell SL, MacDuff DA, Kimmey JM, Diner EJ, Olivas J, Vance RE, Stallings CL, Virgin HW, Cox JS (2015) The cytosolic sensor cGAS detects mycobacterium tuberculosis DNA to induce type I interferons and activate autophagy. *Cell Host Microbe* 17: 811–819

Wu YX, Jin SH, Liu QX, Zhang Y, Ma L, Zhao ZY, Yang S, Li YP, Cui J (2021) Selective autophagy controls the stability of transcription factor IRF3 to balance type I interferon production and immune suppression. *Autophagy* 17: 1379–1392

Xia T, Konno H, Ahn J, Barber GN (2016a) Deregulation of STING signaling in colorectal carcinoma constrains DNA damage responses and correlates with tumorigenesis. *Cell Rep* 14: 282–297

Xia T, Konno H, Barber GN (2016b) Recurrent loss of STING signaling in melanoma correlates with susceptibility to viral oncolysis. *Cancer Res* 76: 6747–6759

Xu YF, Wan W, Shou X, Huang R, You ZY, Shou YH, Wang LL, Zhou TH, Liu W (2016) TP53INP2/DOR, a mediator of cell autophagy, promotes rDNA transcription via facilitating the assembly of the POLR1/RNA polymerase I preinitiation complex at rDNA promoters. *Autophagy* 12: 1118–1128

Yang L, Wang LL, Ketkar H, Ma JZ, Yang G, Cui S, Geng TT, Mordue DG, Fujimoto T, Cheng G *et al* (2018) UBXN3B positively regulates STING-mediated antiviral immune responses. *Nat Commun* 9: 2329

Zhang BC, Nandakumar R, Reinert LS, Huang JR, Laustsen A, Gao ZL, Sun CL, Jensen SB, Troldborg A, Assil S *et al* (2020) STEEP mediates STING ER exit and activation of signaling. *Nat Immunol* 21: 868–879

Zhao YG, Chen Y, Miao G, Zhao H, Qu W, Li D, Wang Z, Liu N, Li L, Chen S *et al* (2017) The ER-localized transmembrane protein EPG-3/VMP1 regulates SERCA activity to control ER-isolation membrane contacts for autophagosome formation. *Mol Cell* 67: 974–989